Received: 27 July 2018 | Revised: 14 December 2018 | Accepted: 21 December 2018

DOI: 10.1002/dep2.57

SPECIAL ISSUE ARTICLE

The Depositional Record Open Access
A journal of the International Association of Sedimentologists
IAS WILEY

A Late Quaternary record of highstand shedding from an isolated carbonate platform (Juan de Nova, southern Indian Ocean)

John W. Counts[1,2] | **Stephan J. Jorry**[2] | **Natalia Vazquez Riveiros**[2] | **Gwenael Jouet**[2] | **Jacques Giraudeau**[3] | **Sandrine Cheron**[2] | **Audrey Boissier**[2] | **Elda Miramontes**[4]

[1]Irish Centre for Research in Applied Geosciences (iCRAG), O'Brien Centre for Science, University College Dublin, Dublin, Ireland

[2]IFREMER, Unité Géosciences Marines —Pointe du Diable, Plouzané, France

[3]UMR CNRS 5805 EPOC—Université de Bordeaux, Pessac Cedex, France

[4]CNRS, UMR6538, Laboratoire Géosciences Océan, Institute Universitaire Européen de la Mer—Université de Bretagne Occidentale (IUEM-UBO), Plouzané, France

Correspondence
John W. Counts, Irish Centre for Research in Applied Geosciences (iCRAG), O'Brien Centre for Science, University College Dublin, Dublin, Ireland.
Email: john.counts@icrag-centre.org

Funding information
TOTAL and IFREMER as part of the PAMELA project, Grant/Award Number: 13/1210499; French government as part of the REEFCORES project; LabexMER, Grant/Award Number: ANR-10-LABX-19; Regional Council of Brittany

Abstract

A 27 m core collected on the sea floor near Juan de Nova island at 1,909 m depth in the SW Indian Ocean preserves a high-resolution record of carbonate sediment export to the deep sea over the past 1 Myr. Core chronology was established using calcareous nannofossil biostratigraphy and benthic foraminiferal $\delta^{18}O$. Throughout the core, preserved highstand intervals (MIS 1, 5, 7, 9, 11, 13, 15, 23 and 25) are marked by an increase in the aragonite content within the sediment. Aragonite is likely sourced from the nearby Juan de Nova carbonate platform *ca* 10 km to the south, and is interpreted as resulting from flooding of the platform top. Platform inundation allows carbonate muds to be winnowed from their original shallow-water environment of deposition, suspended in the water column, and redeposited onto the proximal slopes and within the basin. Sharp increases in aragonite content at the beginning of each highstand interval can be used to estimate the approximate sea-level range when platform flooding occurred; results show that the depth of the platform top has likely changed little over the past 1 Myr due to balanced aggradation and subsidence. Previously hypothesized large-scale aragonite dissolution cycles are evidenced by a disproportionally low aragonite increase during MIS 11. This study provides a new, exceptionally long record of highstand shedding, expanding the known occurrences of the process to the southern Indian Ocean and supporting its importance as a globally significant depositional mechanism that impacts deep-sea stratigraphic records.

KEYWORDS
aragonite, atoll, MIS 11, Mozambique Channel, sea-level change

1 | INTRODUCTION

Unlike terrigenous sediments, carbonates are usually exported to the deep sea in greater abundance during periods of relatively high sea-level. Carbonate content in sediments adjacent to flat-topped platforms has often been seen to increase and decrease proportionally with sea-level change (Chabaud et al., 2016; Paul, Reijmer, Fürstenau, Kinkel, & Betzler, 2012; Reymer, Schlager, & Droxler, 1988), reflecting the production and export of carbonate

during times when the platform top is flooded. This phenomenon (highstand shedding of carbonate platforms; Schlager, Reijmer, & Droxler, 1994) has been documented in both modern-day settings (Andresen, Reijmer, & Droxler, 2003; Betzler, Lüdmann, Hübscher, & Fürstenau, 2013; Droxler, Alley, Howard, Poore, & Burckle, 2003; Droxler, Haddad, Mucciarone, & Cullen, 1990; Droxler & Jorry, 2013; Hine, Wilber, Bane, Neumann, & Lorenson, 1981; Jorry, Droxler, & Francis, 2010; Lantzsch, Roth, Reijmer, & Kinkel, 2007; Paul et al., 2012; Reijmer, Palmieri, & Groen, 2012; Rendle-Bühring & Reijmer, 2005) and in the geological record (Everts, 1991; Reijmer, Ten Kate, Sprenger, & Schlager, 1991; Vecsei & Sanders, 1997). Past studies (Dunbar & Dickens, 2003; Page & Dickens, 2005), however, indicate that mixed systems may be more complicated than the simple highstand shedding model proposed originally by Droxler and Schlager (1985). Because the record of highstand shedding in the modern oceans is generally limited to carbonate platforms and margins in only a few well-studied localities, new information is needed to better understand the carbonate response to sea-level change at a global scale.

Here, we describe for the first time an exceptionally long record of highstand shedding of carbonate mud from Juan de Nova, an isolated, volcano-cored carbonate platform in the southern Indian Ocean. A single 27 m sediment core, collected on the lower seamount rise, records the export of carbonate sediment and the timing of platform flooding over the past 1 Myr in the form of aragonite cyclicity within sea floor muds. This study provides a new, high-resolution example of the highstand shedding concept, validating it as a primary control on sedimentary character and sedimentation rate in this undocumented region of the deep-sea area near carbonate platforms.

2 | BACKGROUND

Juan de Nova island (40 km^2) is the subaerially exposed portion of a small (200 km^2), volcano-cored carbonate platform 135 km off the western coast of Madagascar in the Mozambique Channel (Figure 1a,b). The subaerial island itself (Figure 1c) contains evidence of karstification and erosion of lithified carbonate reefs from the previous highstand (Jorry et al., 2016). The crescent-shaped morphology of the island and the large sand bank on its northern side (red-orange in Figure 1d) are due to the predominance of winds from the south (Figure 1e; Météo France, 2017). The top of the overall platform, ranging between +15 and −30 m water depth, is generally flat and circular (Figure 1d) (Jorry et al., 2016). Sediment on the platform top is lacking in mud, consisting primarily of carbonate sand <2 mm in diameter, composed mostly of the skeletal fragments of calcareous algae (*Halimeda*), Scleractinian corals, molluscs and foraminifers (Jorry et al., 2016). Clastic or volcanic material has not been observed on the platform top.

The submarine flanks of the Juan de Nova volcanic edifice are steep (0–47°, with upper slope generally around 25–35° and steeper on the windward side; Counts, Jorry, Leroux, Miramontes, & Jouet, 2018), reflecting the underlying volcanic nature of the platform. The adjacent basin floor ranges between 2,000 and 2,500 m water depth (Figure 1d). Although platform-derived sediments are intermixed with those from the Madagascar shelf on the deep sea floor, the Juan de Nova island and platform top form a pure carbonate environment. The marine sediment core that is the focus of this study (MOZ4-CS09) lies on the lower slope of the leeward (northern) side of the platform margin in 1,909 m water depth and on a slope of 4.3° inclination (Figure 1d). Further details of slope morphology and sedimentation on Juan de Nova and surrounding areas can be found in Counts et al. (2018).

In the southern and central Indian Ocean, the South Equatorial Current flows at low latitudes from east to west as part of ocean-scale anticyclonic gyres. The island of Madagascar shields the Mozambique Channel (and thus Juan de Nova) from the direct influence of these currents, diverting flow north and south (Northeast and Southeast Madagascar Currents) and creating large eddies that move southwards across the Mozambique Channel (Figure 1a; Schott, Xie, & McCreary, 2009). Surface currents surrounding Juan de Nova island are variable, though in situ measurements show a consistent south to north current direction, with intensities ranging from <20 to more than 100 cm/s near the surface (Figure 1d). The Mozambique Channel is seasonally affected by monsoons; rainfall primarily occurs in the summer months between November and May (Sætre, 1985).

3 | METHODOLOGY

Core MOZ4-CS09 (16°50.802′S, 42°45.440′E) was collected with a Calypso piston coring system by the R/V *Pourquoi Pas?* during the research cruise PAMELA-MOZ04 in 2015 (Jouet & Deville, 2015). Current data around the island were collected by the R/V *L'Atalante* during the PTOLEMEE survey in 2014 with a hull-mounted ADCP (Acoustic Doppler Current Profiler; 150 kHz) and were processed using Cascade 7.1 software. The core was described on board, photographed and analysed with a GEOTEK multisensor core logging system (MSCL) and an AVAATECH energy dispersive X-ray fluorescence (ED-XRF) core scanner every centimetre. MSCL provided bulk density and reflectance data (light/dark value). Semi-quantitative compositional data for various chemical elements, including

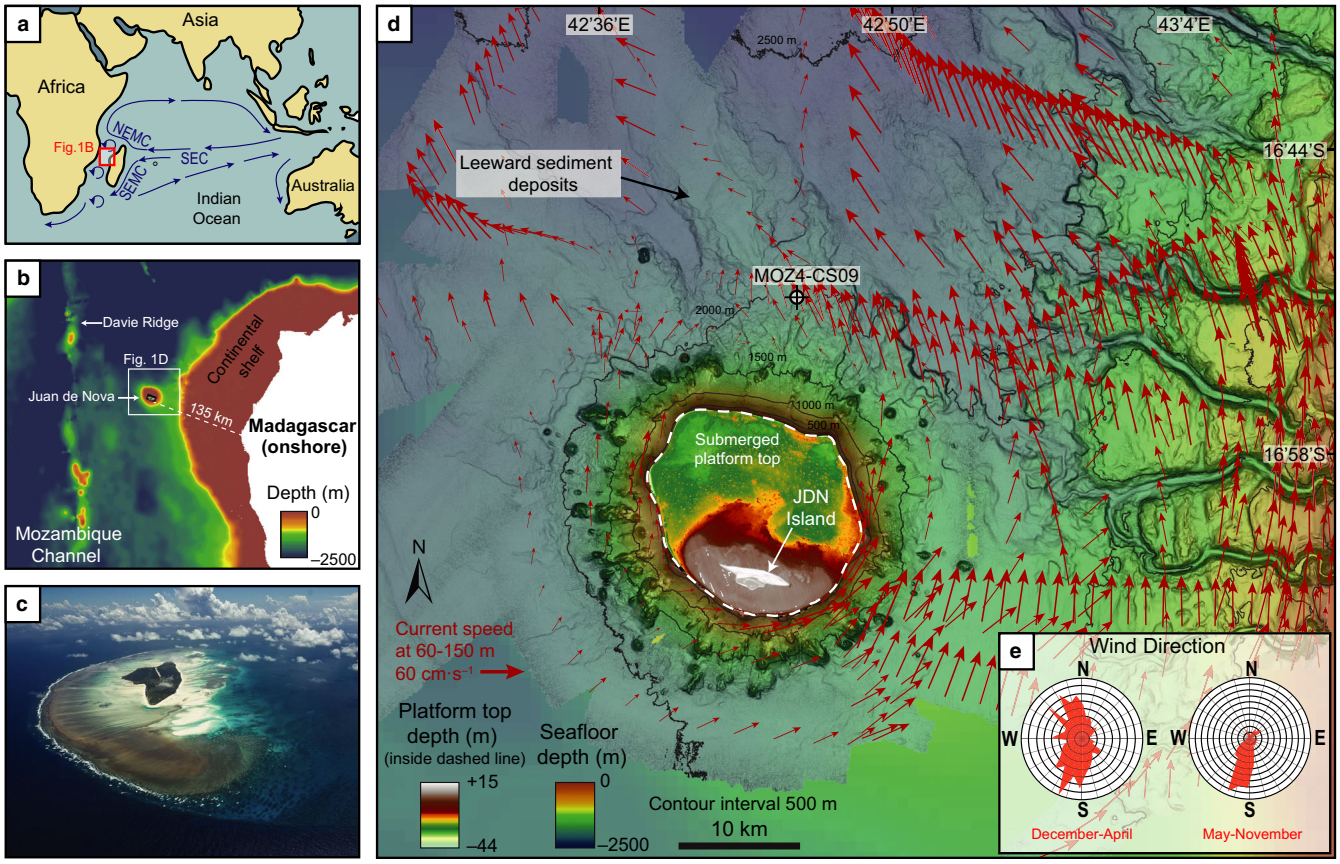

FIGURE 1 Location and background of Juan de Nova platform. (a) Location of study area relative to large-scale currents in the Indian Ocean. Ocean circulation data from Schott et al. (2009). SEC: South Equatorial Current; NEMC: Northeast Madagascar Current; SEMC: Southeast Madagascar Current. (b) Bathymetry of the northeastern Mozambique Channel, showing isolation of Juan de Nova platform from Madagascar shelf. (c) Aerial photo of subaerial and shallow marine portions of Juan de Nova. Modified from Jorry et al. (2016), picture from French Southern and Antarctic Lands (TAAF). (d) Detailed bathymetry of platform top (Lidar data from the Litto3D program), flanks and adjacent sea floor (PTOLEMEE cruise; Jorry, 2014), with superimposed shallow current data (computed from ADCP data, PTOLEMEE cruise; Jorry, 2014). (e) Wind data (490 measurements December–April, 764 measurements May–December; Météo France, 2017) collected from a weather station on the island

strontium (Sr), were provided by ED-XRF. In order to corroborate ED-XRF results, samples were taken in the core every 10 cm for bulk mineralogical composition using X-ray diffraction (XRD) analysis, performed in-house using a Bruker AXS diffractometer. Additional quantification (percentage) of major elements was performed using a Bruker wavelength dispersive XRF (WD-XRF). In order to obtain a higher resolution record of sediment composition over time, aragonite composition from the 130 XRD measurements were compared to the WD-XRF and ED-XRF Sr content measured approximately every centimetre (Chéron, Etoubleau, Bayon, Garziglia, & Boissier, 2016). Strontium is preferentially concentrated in aragonite when it is precipitated in sea water (Schlanger, 1988), and the Ca/Sr ratio in sediment has been used in the past as a proxy for detrital carbonate (Boardman et al., 1986; Chabaud et al., 2016; Hodell, Channell, Curtis, Romero, & Röhl, 2008). Here, Sr and aragonite content showed a highly significant correlation ($r^2 = 0.86$, with a single outlying point removed at 980 cm depth; Figure 2a), with generally <10% deviance between XRD and WD-XRF measurements (Figure 2b). These results indicate that Sr content alone can confidently be used to estimate the aragonite flux over time. Aragonite-enriched and aragonite-deficient intervals in the core were also imaged with a scanning electron microscope to better visualize the nature of lithologic changes.

One centimetre thick sediment samples were taken every 10 cm for extraction of benthic foraminifera. Monospecific *Cibicidoides wuellerstorfi* samples (3–8 individuals per sample, >200 μm, total of 266 samples) were picked and analysed for $^{18}O/^{16}O$ ($\delta^{18}O$ hereafter, expressed in ‰ vs. Vienna Pee-Dee Belemnite, VPDB relative to NBS-19) isotopes at the Leibniz Laboratory for Radiometric Dating and Stable Isotope Research at Kiel University, Germany, using a Kiel IV carbonate preparation device connected to a MAT 253 mass spectrometer from ThermoScientific. Precision of all different laboratory internal and international standards (NBS-19 and IAEA-603) is ±0.09‰. The primary age model was based on correlation of the benthic $\delta^{18}O$ record to the LR04 benthic stack (Lisiecki & Raymo, 2005), using the program AnalySeries (Paillard,

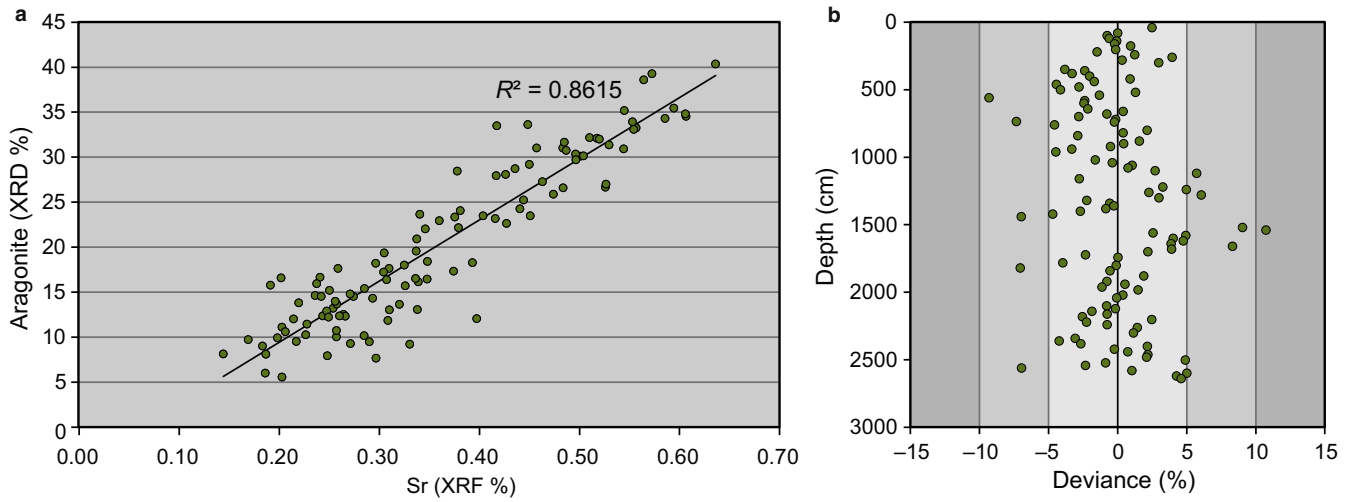

FIGURE 2 (a) Correlation between strontium, as measured in quantitative X-ray fluorescence (XRF), and aragonite, as measured by powder X-ray diffraction (XRD). A single outlying point (from 980 cm depth in the core) removed. R^2 value of the correlation = 0.8615. (b) Deviation of aragonite content derived from XRF Sr data from quantitative XRD measurements, showing <10% variance overall, indicating that XRF data are a reasonable approximation of aragonite content

Labeyrie, & Yiou, 1996). Tie points and error are noted in Table 1; error of tie points is primarily a result of the sampling interval and averages 5.4 kyr. Data used for the age model are available online as a supplementary data set at SEANOE (https://doi.org/10.17882/58006). This stratigraphic framework was further constrained by biostratigraphic data or biohorizons as defined by first and last occurrences of calcareous nannofossil species (Reale & Monechi, 2005; Sato, Kameo, & Takayama, 1991; Thierstein, Geitzenauer, Molfino, & Shackleton, 1977) as well as by dominance intervals within this group of single species/taxonomical categories, which were calibrated to isotopic stages according to Pujos (1988), Weaver (1993), and Giraudeau, Christensen, Hermelin, Lange, and Motoyama (1998). Once the age model was established, the percentage of aragonite in the core (as determined by XRD) was compared to sea-level for a given time interval, rounded to the closest 1 kyr. Sea-level values used were taken from Spratt and Lisiecki (2016) until 800 ka, and from Miller, Mountain, Wright, and Browning (2011) for older dates (mean values). Percentage of aragonite was also compared to the estimated available optimal area for carbonate production on the platform, as determined from bathymetric data on the present-day platform.

TABLE 1 Tie points used to constrain core chronology

MOZ4-CS09 depth (cm)	MOZ4-CS09 age LR04 (kyr)	Error on the age of the pointers (kyr)
13.4	2.000	4.929
75.8	13.342	3.745
581.7	131.897	4.962
751.6	190.570	5.981
861.1	220.006	3.200
957.5	243.815	3.687
1,095.0	288.766	7.762
1,174.3	335.865	3.949
1,349.4	393.288	7.060
1,538.4	425.059	7.976
1,662.4	481.818	5.096
1,779.5	511.975	6.118
1,792.0	553.180	8.377
1,927.9	580.933	2.380
2,014.8	597.916	1.701
2,179.8	618.460	7.059
2,191.0	872.995	9.284
2,353.8	917.335	2.825
2,439.7	937.531	8.850
2,579.0	959.192	3.451
2,627.2	970.865	5.023

Bulk grain sizes of samples from Juan de Nova platform top, collected during shallow marine investigations during the REEFCORES project (2011–2014), were determined by sieving in several size classes from >16 mm down to a minimum of 2 mm. Grain-size analysis throughout the core was carried out with a Malvern Mastersizer 3000 laser diffraction particle sizer, which measured all grains between 10 nm and 2 mm. The coarser grained bed between 3 and 4 m depth was selected for further analysis—a sample of several grams was split and sieved at three different size fractions (0.063–0.5 mm, 0.5–1 mm and 1–2 mm). Each fraction was further split, and *ca* 300 grains per size class were examined under a binocular microscope to determine their origin, using Milliman, Müller, and Förstner (1974) as a guide for identification. Elsewhere in the core, presumed unconformities in muds were sampled for thin sections. These were vacuum

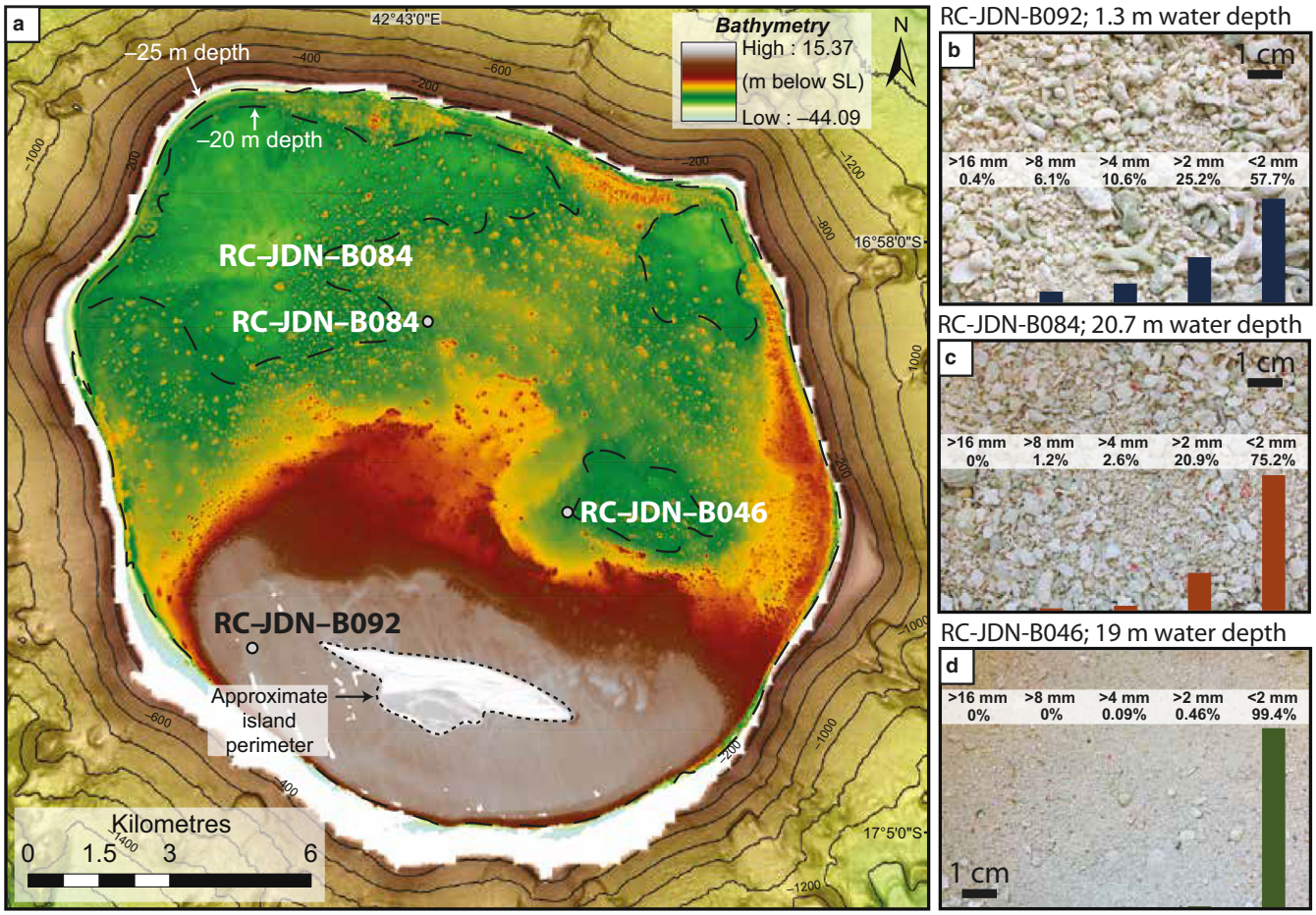

FIGURE 3 (a) High-resolution LIDAR bathymetry and topography of Juan de Nova island and platform top, and swath bathymetry around the seamount. Location of sediment samples in b–d labelled. (b–d) Representative sediment samples and grain-size data from the platform top

impregnated with blue epoxy and prepared at the University of Bordeaux. Muds in the core were also imaged in-house at Ifremer using an FEI Quanta 200 scanning electron microscope.

Mass accumulation rates of aragonite (MAR_{ar}; g cm^{-2} kyr^{-1}) were calculated using the methodology of Jorry et al. (2010):

$$MAR_{ar} = wt\%_{ar} \times LSR \times \rho_{db},$$

where $wt\%_{ar}$ is the weight percent aragonite, as determined by XRF core scanner, LSR is the linear sedimentation rate (cm/kyr) and ρ_{db} is the dry bulk density (g/cm^3) (Jorry et al., 2010). ρ_{db} was calculated by removing the density of water from pore space:

$$\rho = \rho - (FP \times \rho_w),$$

where ρ_b is the bulk density, FP is fractional porosity and ρ_w is the density of water. ρ_b was directly measured on the core onboard the RV *Pourqoui Pas?* using a MSCL, and FP was directly calculated from these bulk density measurements.

The potentially productive area of the platform top was calculated for various hypothetical sea-levels by generating smoothed bathymetric contours on the high-resolution Lidar grid shown in Figure 3a. As this data set merged with the lower resolution deeper bathymetric data at the platform top margin, the uppermost part of the slope did not have continuous coverage. Calculated areas in the upper slope therefore were estimated using a simple geometric model and projecting the slope gradient out laterally from the areas where data were acquired, leading to similar values for depths below 60 m. Calculated areas should therefore be regarded as reasonable approximations.

4 | RESULTS

4.1 | Sedimentology of the platform top and adjacent sea floor

The platform top contains numerous metre-scale patch reefs in its interior and a discontinuous fringing reef along the northern margin (Figure 3a). Samples taken on the platform top (water depths between 1 and 21 m; locations shown in

Figure 3a) were examined for comparison with deep-sea sediments in core. Sediment composition on the platform top is relatively coarse, consisting almost entirely of carbonate sand and gravel in the form of aragonitic skeletal fragments (Figure 3b–d). Detailed results of platform top sediment composition can be found in Jorry et al. (2016).

On the adjacent deep sea floor, core MOZ4-CS09 consists almost entirely of muds (Figure 4a) containing abundant planktonic foraminifera and variable proportions of carbonate and siliciclastic minerals. Except for carbonate sand layers in the upper part of the core, the dominant grain size over the entire 27 m length is <20 μm, although the tests of foraminifers may reach sand-size (63 μm–2 mm). Despite the apparent lithological homogeneity, compositional variations in the mud are evidenced by quantifiable colour changes (Figure 4a). The XRD and WD-XRF data (Figure 2) reveal that these cyclic colour changes correspond to changes in the aragonitic content within the mud, with lighter colours containing proportionally more aragonite than darker, browner intervals. Increases in aragonite abundance were easily discernible in SEM images by the presence or absence of micron-scale needle-like crystals within the sediment (Figure $4b_1$, 448 cm depth). In places, these needles show evidence of dissolution and pitting (Figure $4b_2$, 1,410 cm depth). Elsewhere, where XRF/XRD data showed aragonite to be less abundant, sediment consisted primarily of platy clay minerals (Figure $4b_3$, 600 cm depth), identified as silicate clays by EDS analysis (Counts et al., 2018). While these clay-rich intervals are found on the sea floor adjacent to the platform, the clastic material likely does not originate from the platform itself, which at present only contains carbonate sediment.

Discrete beds of carbonate sand are relatively rare in the core, with only one (from 319 to 337 cm) reaching a significant thickness. Grain size in this bed fines upward overall, although grains are consistently between 0.42 and 0.43 mm in diameter (medium sand) for a 10 cm interval in the bed centre (Figure 4c). Sand-sized grains in this bed are almost all skeletal fragments, predominantly consisting of calcareous algae, corals and both benthic and planktonic foraminifers. This composition is size-dependent: foraminifers make up an increasingly higher proportion at finer fractions (Figure 4d). This bed and others like it have previously been interpreted as the product of turbiditic events, ultimately originating from the platform top (Counts et al., 2018), but likely incorporating slope material during downslope movement.

4.2 | Core chronology

The age model reveals that the upper *ca* 18 m of core sediments are a continuous record spanning approximately the last 500 kyr, back to MIS 13 (Figure 5). In this section of the core, isotope data closely match the LR04 stack. The stratigraphic framework for the upper part of the core is also confirmed by the presence of key datums (*Emiliania huxleyi*, *Pseudoemiliania lacunosa* and *Reticulofenestra asanoi*) as well as dominance changes within the *Gephyrocapsa* species group (Table 2). Below this point, an age model compatible with both the LR04 stack and the nannofossil data required the placement of two unconformities in the lower part of the core, one from 513 to 50 ka (MIS 13–14), and a much larger one between 623 and 872 ka (MIS 16–21). Both of these unconformities coincide with a sharp change in sediment colour (lighter grey vs. darker brown), which represents a change in the composition of the finest sediment fraction. Unconformities could also be seen in thin section to be characterized by differences in abundance of planktonic foraminifera, with increased abundance below the unconformity in both cases (Figure 6). The shorter, shallower unconformity (Unconformity 1) was not a result of biostratigraphic constraint; its placement was based instead on the absence of the second, isotopically lighter peak at the end of the MIS 13 interglacial interval. However, the age of sediments between *ca* 18 and 22 m is confirmed to be around MIS 15–16 based on the presence of *P. lacunosa*, the absence of *R. asanoi*, and the transition between the *G. caribbeanica* and the small *Gephyrocapsa* acme zones (Weaver, 1993). The deeper unconformity (Unconformity 2) lasted much longer, spanning *ca* 250 kyr. This duration is the result of both biostratigraphic restrictions and best-fit matching of the isotope ratio curve. Most notably, the simultaneous presence of dominant small forms of *Gephyrocapsa,* and of common *P. lacunosa* and *R. asanoi* coccoliths in a sample taken at 2,372 cm depth constrains this interval to MIS 23–25. The dominance of *G. caribbeanica* together with the common occurrence of *P. lacunosa* and *R. asanoi* near the bottom of the core further constrains the age of the oldest sediments retrieved as between MIS 25 and MIS 30 (*ca* 0.94–1 Ma). (Table 2). The age model shown in Figure 5 is therefore the most parsimonious interpretation of the two independent data sets: isotopes and nannofossil biostratigraphy.

FIGURE 4 Sedimentology of core MOZ4-CS09. (a) Core properties, including lithology, colourimetry (light/dark value) and core photos, gamma density (g/cm^3), grain-size (μm) measurements, and benthic δ^{18}O isotopic values (per mil Vienna Pee-Dee Belemnite) and position of samples used for nannofossil determination and SEM and grain-size analyses. (b) SEM images of core sediments, showing abundant needle-like crystals of aragonite at depths 448 and 1,410 cm, and platy clay minerals at 600 cm. (c) Quantitative grain-size information for the carbonate sand bed between 320 and 340 cm. (d) Compositional data for sands from the interval 338–340 cm, the base of the bed shown in (c). A total of 855 individual grains of three size classes were analysed for taxonomic affiliation, with identification aided by Milliman, Müller, and Förstner (1974)

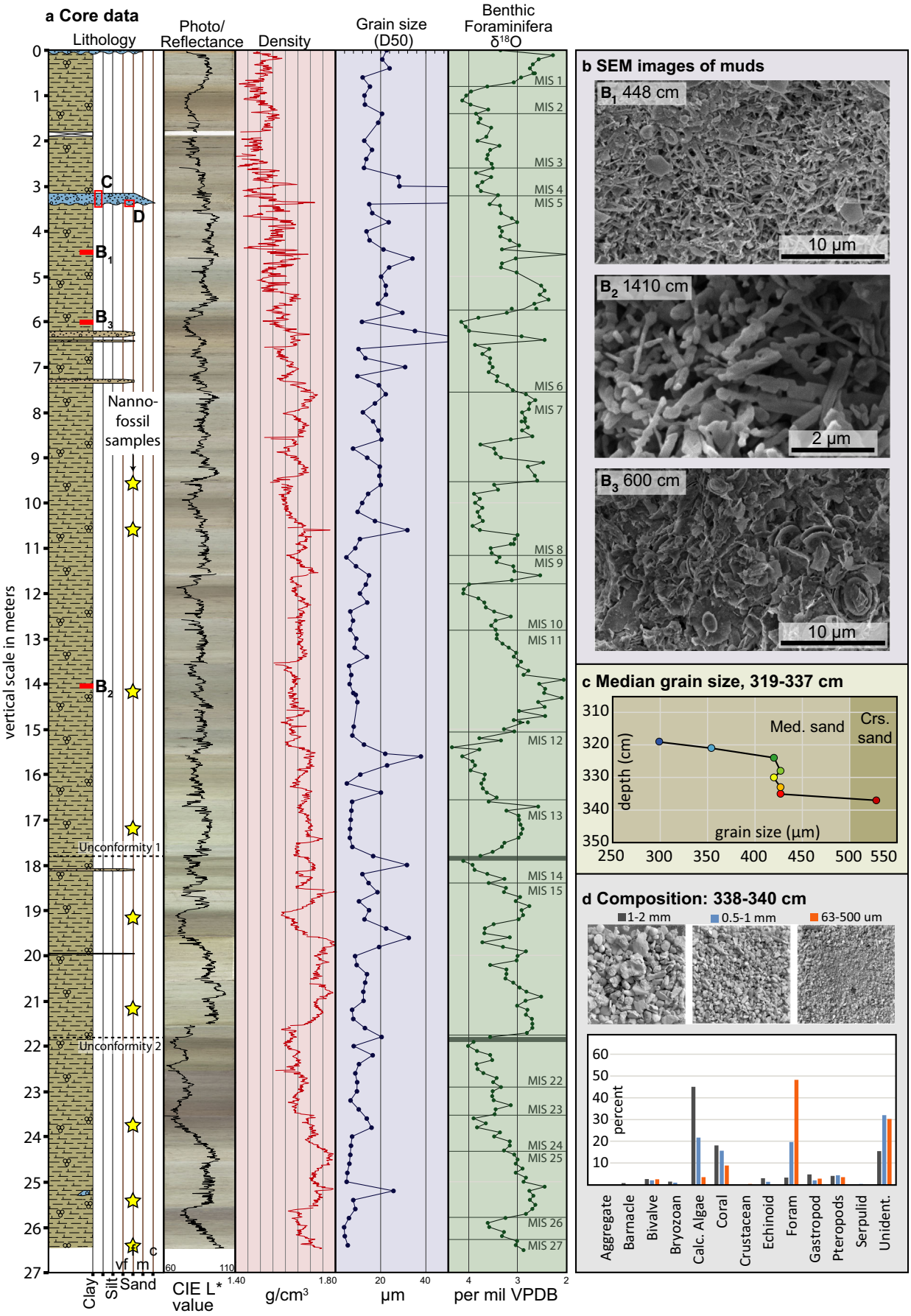
a Core data
Lithology
Photo/ Reflectance
Density
Grain size (D50)
Benthic Foraminifera δ18O
vertical scale in meters
C
D
B1
B3
B2
Nanno-fossil samples
Unconformity 1
Unconformity 2
MIS 1
MIS 2
MIS 3
MIS 4
MIS 5
MIS 6
MIS 7
MIS 8
MIS 9
MIS 10
MIS 11
MIS 12
MIS 13
MIS 14
MIS 15
MIS 22
MIS 23
MIS 24
MIS 25
MIS 26
MIS 27
Clay
Silt
Sand
vf f m c
CIE L* value
g/cm3
µm
per mil VPDB
b SEM images of muds
B1 448 cm
10 µm
B2 1410 cm
2 µm
B3 600 cm
10 µm
c Median grain size, 319-337 cm
depth (cm)
grain size (µm)
Med. sand
Crs. sand
d Composition: 338-340 cm
1-2 mm
0.5-1 mm
63-500 um
percent
Aggregate
Barnacle
Bivalve
Bryozoan
Calc. Algae
Coral
Crustacean
Echinoid
Foram
Gastropod
Pteropods
Serpulid
Unident.

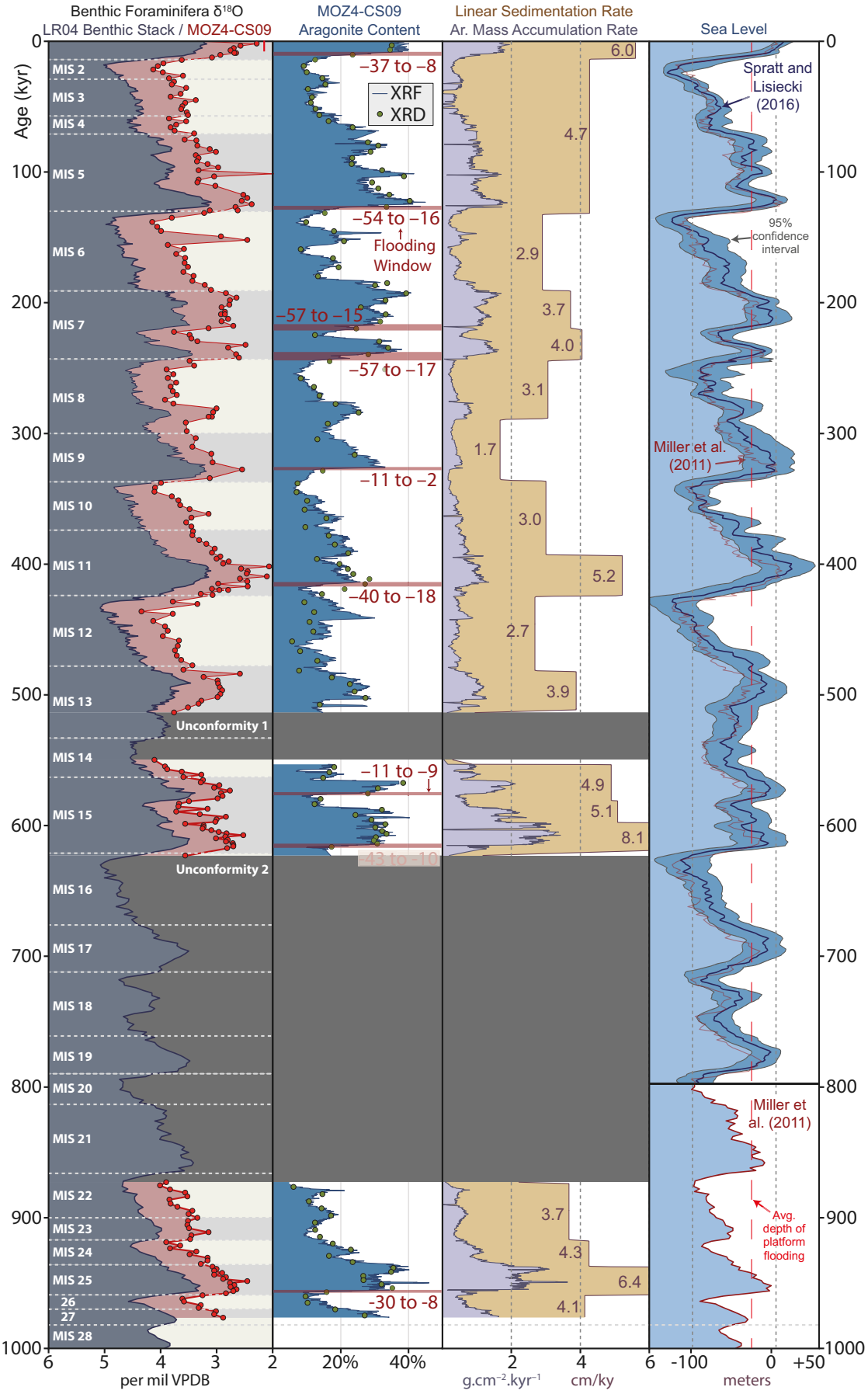
Benthic Foraminifera δ18O
LR04 Benthic Stack / MOZ4-CS09
MOZ4-CS09
Aragonite Content
Linear Sedimentation Rate
Ar. Mass Accumulation Rate
Sea Level
Age (kyr)
MIS 2
MIS 3
MIS 4
MIS 5
MIS 6
MIS 7
MIS 8
MIS 9
MIS 10
MIS 11
MIS 12
MIS 13
Unconformity 1
MIS 14
MIS 15
Unconformity 2
MIS 16
MIS 17
MIS 18
MIS 19
MIS 20
MIS 21
MIS 22
MIS 23
MIS 24
MIS 25
26
27
MIS 28
XRF
XRD
−37 to −8
−54 to −16
Flooding Window
−57 to −15
−57 to −17
−11 to −2
−40 to −18
−11 to −9
−43 to −10
−30 to -8
6.0
4.7
2.9
3.7
4.0
3.1
1.7
3.0
5.2
2.7
3.9
4.9
5.1
8.1
3.7
4.3
6.4
4.1
Spratt and Lisiecki (2016)
95% confidence interval
Miller et al. (2011)
Miller et al. (2011)
Avg. depth of platform flooding
per mil VPDB
g.cm−2.kyr−1
cm/ky
meters

FIGURE 5 Age model of the core, based on correlation with the LR04 benthic stack (Lisiecki & Raymo, 2005). Column 1: Benthic $\delta^{18}O$ isotope (‰Vienna Pee-Dee Belemnite). MIS boundaries (Cohen & Gibbard, 2008) and unconformities (1,780–1,784 cm/513–550 ka and 2,180–2,186 cm/623–872 ka) are marked. Column 2: Aragonite content (%), as measured by both X-ray fluorescence and X-ray diffraction. Note convergence of the two methods. Interpreted platform flooding windows highlighted in red. Column 3: Linear sedimentation rates (cm/kyr) and aragonite mass accumulation rates (MAR_{ar}, g cm^{-2} kyr^{-1}) for the core. Column 4: Reference sea-level curves from Spratt and Lisiecki (2016) and Miller et al. (2011). Both curves generated from global composites of $\delta^{18}O$ isotope data; Spratt and Lisiecki (2016) only extends back to 800 ka

TABLE 2 Summary of nannofossil data used in creation of the age model

Depth (cm)	Nannofossil marker species	Age constraints
960	Acme zone of Small *Gephyrocapsa*—common to rare *Emiliania huxleyi*	MIS 6–8
1,060	Acme zone of Small *Gephyrocapsa*—common to rare *E. huxleyi*	MIS 6–8
1,417	Acme zone of *G. caribbeanica*—absence of *E. huxleyi*	MIS 9–11
1,719	Acme zone of *G. caribbeanica*—rare to common *Pseudoemiliania lacunosa*	MIS 12–15
1,920	Transition between acme zones of *G. caribbeanica* and small *Gephyrocapsa*—rare to common *P. lacunosa*—absence of *Reticulofenestra asanoi*	MIS 15
2,116	Acme zone of Small *Gephyrocapsa*—rare to common *P. lacunosa*—absence of *R. asanoi*	MIS 15–23
2,372	Acme zone of Small *Gephyrocapsa*—rare to common *P. lacunosa*—rare to common *R. asanoi*	MIS 23–25
2,542	Acme zone of *G. caribbeanica*—common *P. lacunosa*—common *R. asanoi*	MIS 25–30
2,650	Acme zone of *G. caribbeanica*—common *P. lacunosa*—common *R. asanoi*	MIS 25–30

Note. Each row is one sample analysed.

4.3 | Aragonite cycles and sea-level

The comparison of the benthic $\delta^{18}O$ record and the aragonite content shows a clear, direct relationship (Figure 5). Isotopically lighter intervals (interglacial periods, i.e. MIS 1, 5, 7, 9, 11, 13, 15, 23 and 25) correspond in almost every instance to increased aragonite content relative to intervening stages (MIS 2–4, 6, 8, 10, 12, 14, 22, 24, and 26). Although this relationship holds up across multiple glacial–interglacial cycles, the rapid increases in aragonite content consistently lag behind the initial lightening of isotope ratios by several thousand years (Table 3). Since MIS are tied to eustatic rise and fall, variations in aragonite content in the core can be correlated directly to global sea-level magnitude and timing, generally increasing in conjunction with sea-level rise, and decreasing correspondingly with sea-level fall (Miller et al., 2011; Spratt & Lisiecki, 2016; Figure 5). Holocene sea-level curves generated specifically for the western Indian Ocean (Camoin, Montaggioni, and Braithwaite, 2004; Zinke et al., 2003) generally overlap with the composite curves shown in Figure 5, and also correlate well with the most recent (MIS 1–2) aragonite increase. When the percentage of aragonite in the core (all data, as measured by XRD) is cross-plotted against the sea-level for a given age, the relationship can be seen to hold, with an R^2 value of 0.411 (Figure 7a). Marine isotope stages can also be differentiated, with glacial stages clustering together due to their overall lower aragonite content.

To filter out other factors that may influence aragonite content, the relationship between aragonite and sea-level was also examined only during the short periods at stage transitions (Figure 7b), where both aragonite and sea-level are rapidly increasing. These intervals show an aragonite/sea-level relationship that is much more robust ($R^2 = 0.714$) compared to that when all data are included. If this relationship is applied to the whole core to create a curve predicting the expected aragonite content at a given sea-level (blue curve in Figure 7c), the actual aragonite values (orange curve in Figure 7c) can be seen to deviate substantially from the expected relationship during certain intervals. These exceptions often take the form of abnormally low aragonite content during periods of high sea-level (blue shading in Figure 7c). In particular, this is seen during MIS 9, 11, and 12–13, but is best exemplified during Stage 11. During this period, which is characterized by exceptional warmth and high sea-levels (Droxler et al., 2003), aragonite content is, on average, lower than all other interglacial periods observed, and is substantially less than predicted by the relationship shown in Figure 7b.

4.4 | Sedimentation and mass accumulation rates

Due to the construction of the core chronology (benthic $\delta^{18}O$ correlation to the LR04 benthic stack), bulk LSR are necessarily consistent between tie points (Table 1), with values ranging from 1.7 to 8.1 cm/kyr (Figure 5). These values, while variable, are in line with Quaternary sedimentation rates on carbonate slopes and proximal basins in other regions (e.g. periplatform ooze sedimentation rates reported by Droxler & Schlager, 1985). MAR_{ar} range from 0 to 3.6 g

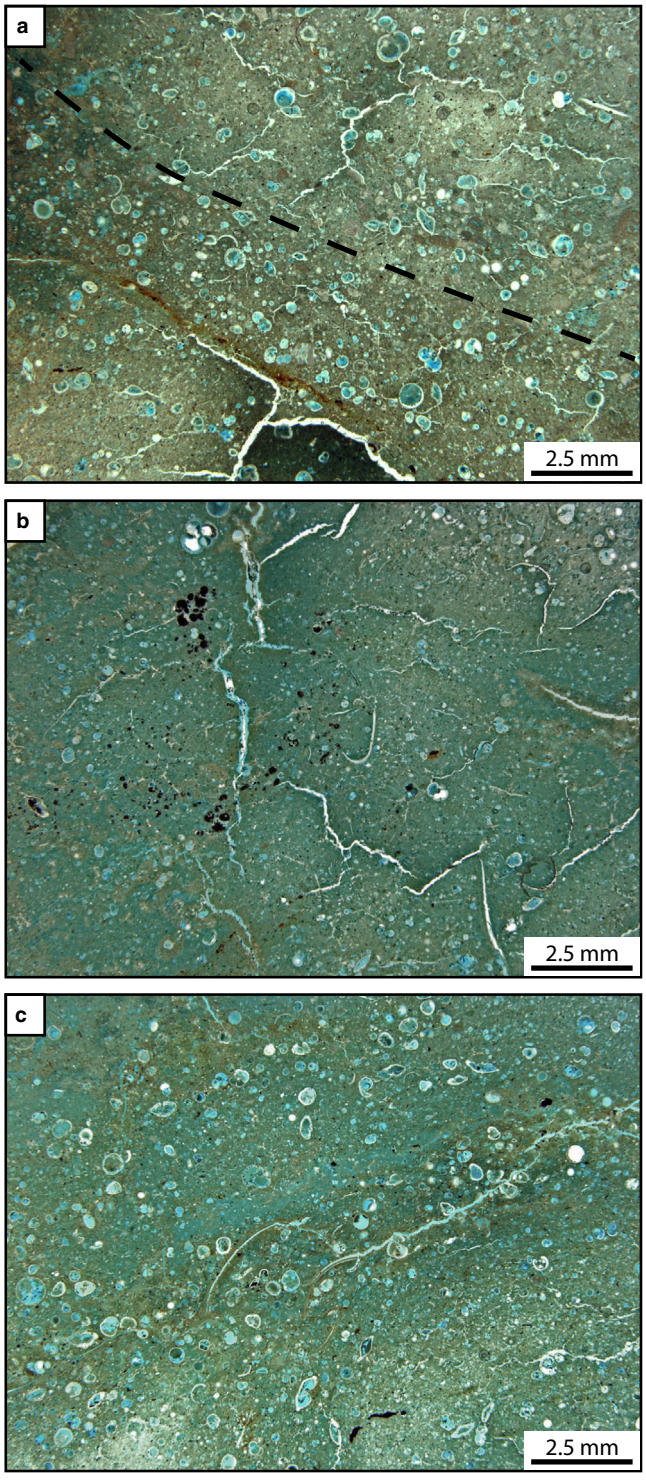

FIGURE 6 Thin sections of sediments adjacent to proposed unconformities. All sections vacuum impregnated with blue epoxy. (a) Section centred around 1,785 cm depth (upper unconformity) showing contact between two sediment types marked by dashed line. (b) Sediment just above lower unconformity, 2,182 cm depth, showing sediment dominated by fine-grained mudstone with few planktonic foraminifers. (c) Sediment just below lower unconformity, showing increase in foraminifer content relative to b). Same scale on all images

TABLE 3 Graphically measured time offset between the decrease in $\delta^{18}O$ isotope ratios and the subsequent initial rapid increase in aragonite content at the onset of selected deglaciations

Stage transition	Aragonite-isotope offset (in years, *ca*)
MIS 1–2	2,500
MIS 5–6	5,000
MIS 7–8	3,100
MIS 9–10	8,200
MIS 11–12	10,900
MIS 15 (younger)	5,000
MIS 15 (older)	5,000
MIS 25–26	3,300

Note. Exact times vary based on where the exact position of the comparison is made; values are therefore approximate.

cm^{-2} kyr^{-1}. Like aragonite content, both LSR and MAR_{ar} show a relationship with sea-level: in general, both increase during highstand (mean *ca* 4.8 cm/year) and decrease during lowstand (mean *ca* 3.5 cm/year), with both curves rising and falling at approximately the same times. The pattern of MAR_{ar} change also generally follows the aragonite content curve, though MAR_{ar} for a given interval may be strongly affected by the LSR. The primary example of this occurs during MIS 9, when aragonite content is as high as other highstand intervals, but both the LSR and the MAR_{ar} are substantially lower than other times when sea-level maxima were of similar magnitude (e.g. MIS 5, when sea-level was within a few 10s of metres; Dutton et al., 2009, 2015).

5 | DISCUSSION

5.1 | Origins of aragonite cyclicity

The relationship described here between aragonite content, accumulation rate and past sea-level change is consistent with the depositional mechanism of highstand shedding, where carbonate sediments are exported off of flat-topped platforms and into the deep sea during times when the platform is inundated by sea water (Schlager et al., 1994). Export is believed to be through winnowing and off-platform transport in suspension and subsequent fallout; there is no evidence for dilute gravity flows in most of the fine-grained muds that form the majority of the core. The aragonite muds described here are interpreted as originating from the shallow-water top of the Juan de Nova platform, where they are precipitated inorganically in supersaturated sea water (Macintyre & Reid, 1992; Milliman, Freile, Steinen, & Wilber, 1993), biogenically in the skeletons of organisms where they begin as larger particles and subsequently break down (Conrad Neumann & Land, 1975), or mechanically/chemically through the feeding and digestive

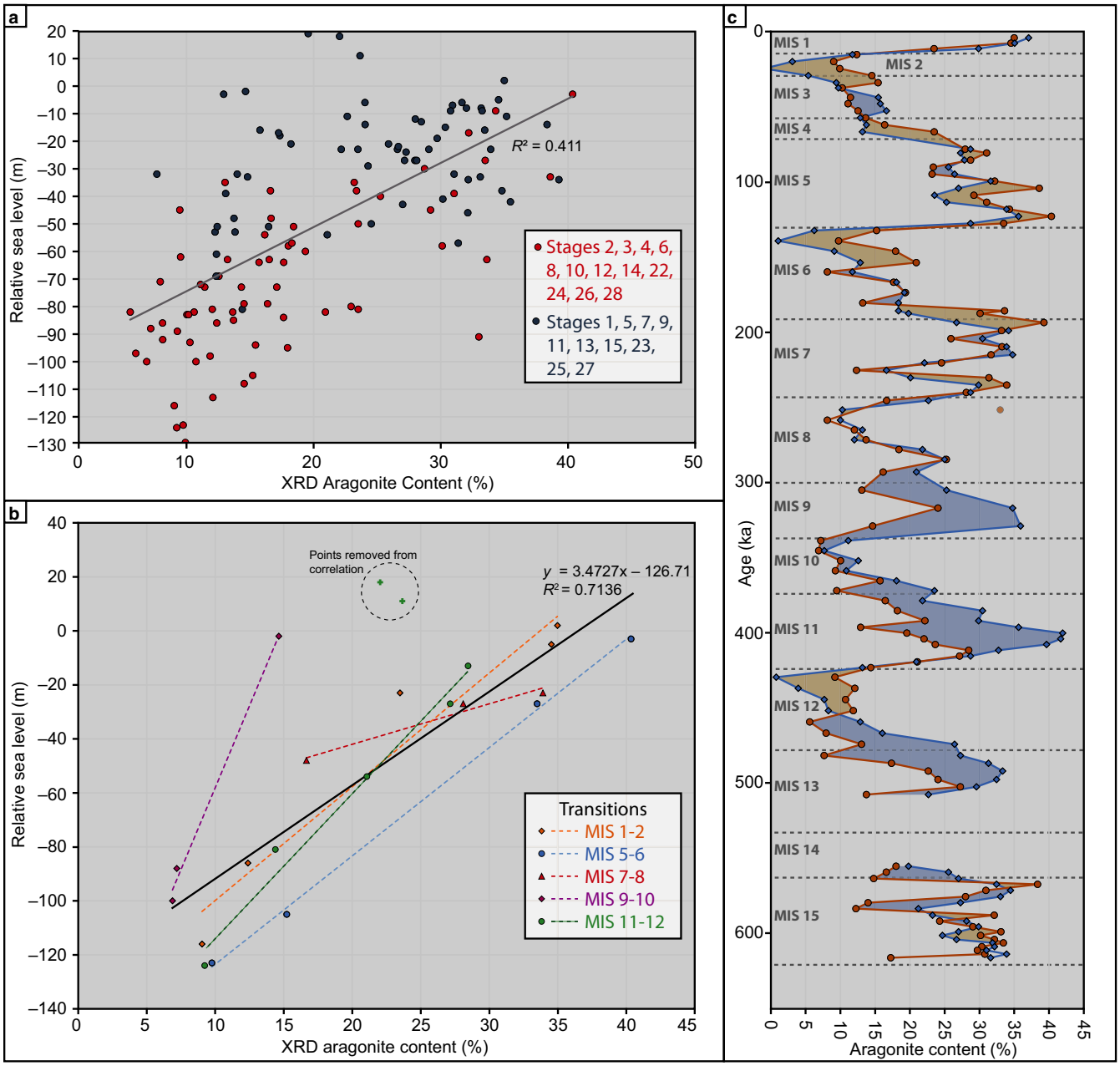

FIGURE 7 (a) Cross-plot of sea-level and aragonite content as determined from X-ray diffraction (XRD) analysis. All data points shown. Stage boundaries from Cohen and Gibbard (2008). (b) Cross-plot of aragonite and sea-level during selected glacial–interglacial transitions, shown in legend. (c) Plot of actual aragonite content (orange line, derived from XRD) and aragonite content as predicted by the relationship calculated in Figure 4b (blue line). Shading indicates the line with greater values

processes of fish (Perry et al., 2011; Salter et al., 2018). Core MOZ4-CS09 lies only 10.5 km from the platform margin, well within the range that fine-grained sediment could be transported by wind or tide-generated currents, or by density cascading processes (Jorry et al., 2016; Wilson & Roberts, 1995). MAR_{ar} and aragonite percentages in core muds often decrease gradually after the initial rise at the beginning of highstand; this may be due to autocyclic processes (e.g. the growth of fringing reefs) that store sediment on the platform top and form barriers to export (Boardman et al., 1986). The initial drop in sea-level following the initial transgression may also disrupt the carbonate factory, reducing exported sediment volumes. Thus, the relationship seen during transitions represents the highstand shedding response before the initiation of these other, secondary factors that affect carbonate volume on the sea floor. The correlation between MAR_{ar} and bulk LSR suggests that LSR increase during highstand is driven by the increase in aragonite, showing that the aragonite content variation through time is not simply the result of changing

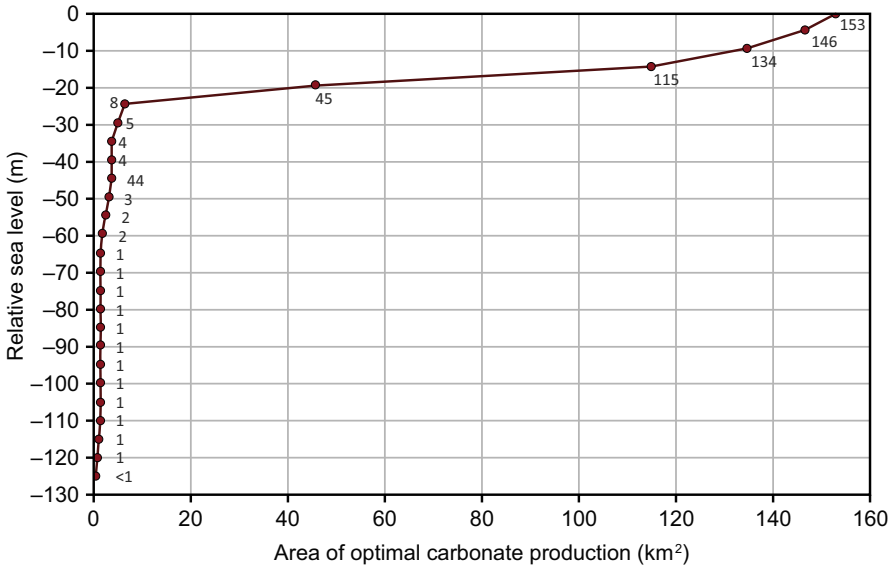

FIGURE 8 Relationship between sea-level and the area available for optimal carbonate productivity, defined here as water depths of 20 m or less. Values rounded to nearest km^2

amounts of clastic dilution. Rather than replacing some component of non-aragonitic sediment, the aragonitic fraction is added to the deposit.

Although the winnowing mechanism plays a substantial role in sediment export, some part of the aragonite response is probably also due to increased carbonate productivity on the platform top (Paul et al., 2012). During glacial lowstands, only the steep flanks of the platform would be submerged, resulting in substantially less area in the shallow photic zone where most carbonate is produced. Inundation of the platform top during interglacials, however, would result in a substantial increase in the area available for carbonate productivity. Bosscher and Schlager (1992) and Glaser and Droxler (1991) note that carbonate reef growth is highest at depths of <20 m, so this depth is used here as an estimate of optimal carbonate productivity for varying sea-levels from 0 to −130 m relative to the present (Figure 8). Such calculations assume a platform morphology similar to that of the present day, and present uncertainties for each variable, including the fact that production may also occur at deeper depths. However, they may provide a first approximation of sea-level related changes in carbonate production. The results show that flooding of the flat platform top may lead to over 150 km^2 available for optimal carbonate production, but the relatively steep slopes below the margin (up to 45° on the lower margin/upper slope) have up to an order of magnitude smaller productive area, with a minimum of *ca* 1 km^2 of space available for carbonate production. It is unlikely that the subaerially exposed platform top itself would generate any substantial volume of fine-grained carbonate, as freshwater cementation may result in rapid induration of exposed sediment (Dravis, 1996) that may later dissolve through karst formation. Similar differences in potential productive area were found by Glaser and Droxler (1993) in the Caribbean Walton Basin. The increased rate of flux of aragonite to the deep sea floor, as seen in the MAR_{ar} shown in Figure 5, is therefore a combination of both a depositional mechanism and increased sediment supply.

Because the modern-day platform is inundated, highstand shedding processes are likely currently operating on Juan de Nova, with mud generated and exported through the processes discussed above. This is confirmed by sedimentological observations on the platform top: sediments are composed primarily of aragonite, and little or no mud is currently preserved, despite the presence of organisms with aragonitic skeletons. The process may be occurring elsewhere in the region—on the top of nearby Glorieuses platform (around 780 km to the northwest), aragonitic muds are also not preserved, and have been hypothesized to have been winnowed into the adjacent basin there as well (Prat et al., 2016). The clastic component of mud on the deep sea floor likely originates from nearby continental shelves, where river systems in Madagascar deposit large volumes of clastic sediment (Fontanier et al., 2018). The finest fraction of these sediments may be transported far offshore in suspension, where they are subsequently deposited as hemipelagic fallout. Numerous canyons (visible in Figure 1d) incise the Madagascar slope and provide further evidence of sediment transport from the island. Shallow current data (Figure 1d) show currents originating from the south/south-west, resulting in a current shadow on the north side of the island where the core was collected. Sediments deposited in this area are therefore likely protected from the effects of deep contour currents; evidence for substantial bottom current modification (sediment waves, contourite drifts, scours, etc.) are not seen in the bathymetric data collected.

5.2 | Platform flooding windows

Jorry et al. (2010) introduced the concept of "re-flooding windows" to denote the interval during which flat platform

tops are inundated during the glacial–interglacial transitions. This concept can also be applied here on a longer timescale by examining sea-level at the onset of intervals of aragonite production. In Juan de Nova, aragonite content generally matches the pattern of sea-level change, that is, a rapid rise at the onset of interglacial stages, and a gradual decrease during subsequent regressions. In most cases, however, the rate of aragonite increase is sharper than the rate of sea-level rise. The window during which this sharp increase occurs is interpreted as coinciding with the flooding of the relatively flat platform top, and to mark the onset of the highstand shedding process. This occurs most clearly at the onset of interglacial conditions in MIS 1, 5, 7, 9, 11, 15 and 25 (labelled in Figure 5; numbers represent sea-level values at the onset and termination of rapid aragonite increase). If the spike in aragonite production during these intervals can be assumed to represent the moment of platform flooding, in all of these instances the flooding event happened when sea-level was between 57 and 2 m below its current level (Figure 5). The average depth of the onset of flooding is 36.7 m, and the average depth where aragonite production stops increasing is 12.4 m. The mean depth of platform flooding is thus 24.6 m, very close to the predominant depth of the current platform top, which is submerged to between 10 and 30 m (Jorry et al., 2016).

While some uncertainty necessarily exists with the core chronology, sea-level reconstructions, and the exact placement of the flooding window, the agreement between these estimates supports the idea that the subsea height of the platform top during these periods was not substantially different from its current state. Substantial aggradation over the past *ca* 1 Myr, if not balanced by subsidence, would have resulted in flooding windows that trended lower than current values. Substantial net subsidence of that platform can be excluded as well, as the presence of highstand shedding necessarily indicates a submerged platform, and sea-level values have only exceeded the current highstand by few metres at most for short periods over the past several sea-level cycles. It is therefore inferred that aggradation and subsidence have been equally matched over most of the Late Quaternary, and the relative height of the platform has stayed much the same as subsidence and deposition have kept pace. Although no direct measurements of tectonic subsidence or uplift have been reported from Juan de Nova., Camoin, Montaggioni, and Braithwaite (2004) note subsidence rates for several other islands in the region (based on Eemian reef terrace data), which range from 0.03 to 0.25 mm/yr. These values are comparable to sedimentation rates compiled for several other Holocene shallow-water carbonate systems (e.g. 0.5–2 mm/yr for bioclastic shoals; Strasser & Samankassou, 2003), demonstrating that sedimentation could have easily kept pace with any ongoing platform subsidence. Courgeon et al. (2016) estimate the rate of subsidence for the nearby Glorieuses platform at 0.01–0.015 mm/yr, in line with these other estimates.

5.3 | Aragonite dissolution cycles

The cyclical, sawtooth pattern of sea floor aragonite content near carbonate platforms has also been observed elsewhere in the world, with alternative mechanisms proposed for its origin. Reymer et al. (1988) observe that the aragonite content in a core from the Bahamas correlates well to small-scale changes in the $\delta^{18}O$ curve, suggesting that these small-scale changes are unlikely to be the result of simple export variations related to flooding and exposure of the platform. They propose that the coupling between the two curves may be due to the dissolution of metastable aragonite on the sea floor, a process tied to sea-level and climate. In other examples (Droxler, Schlager, & Whallon, 1983; Emmermann, 2000), the aragonite response has also been hypothesized to be at least partially the result of climate-related dissolution rather than changes in the amount of carbonate exported. In these studies, evidence for dissolution during glacial periods is partially in the form of a time offset between the relative aragonite increase and the lightening of $\delta^{18}O$ isotope values, where the dissolution ceases and the apparent increase in aragonite precedes sea-level rise and platform flooding by several thousand years, suggesting that export was not at work. In the core studied here, the opposite is the case—aragonite content increases usually occur several thousand years after the initial sharp change in $\delta^{18}O$ values (Table 3). Although there is some range of error in the age model, the pattern of aragonite increase lagging behind sea-level rise is consistent across several cycles, and is thus more in line with the increased production and export of sediment after bank-top flooding rather than glacial–interglacial scale cycles of deep-sea dissolution. Additionally, the overall sedimentation rates in core MOZ4-CS09 tend to increase during highstand intervals (Figure 5), supporting the idea that the bulk input of aragonite to the sea floor is changing cyclically. Sepulcre, Durand, and Bard (2017) note that bioturbation can also lead to an offset between the fine fraction of sediment and the foraminiferal $\delta^{18}O$ record. The precise magnitude of the offset in the Juan de Nova core may therefore have been different than what is currently observed, and caution should therefore be used when attempting to quantify this offset in order to assign a definitive cause to this type of sedimentary response to sea-level change.

Larger scale aragonite supercycles that span multiple glacial–interglacial cycles have also been proposed (Droxler et al., 1990). These cycles of carbonate dissolution are proposed to operate at a larger wavelength (100s of kyr) than the glacial–interglacial dissolution cycles discussed above. The minima of the most recent cycle is centred in MIS 11,

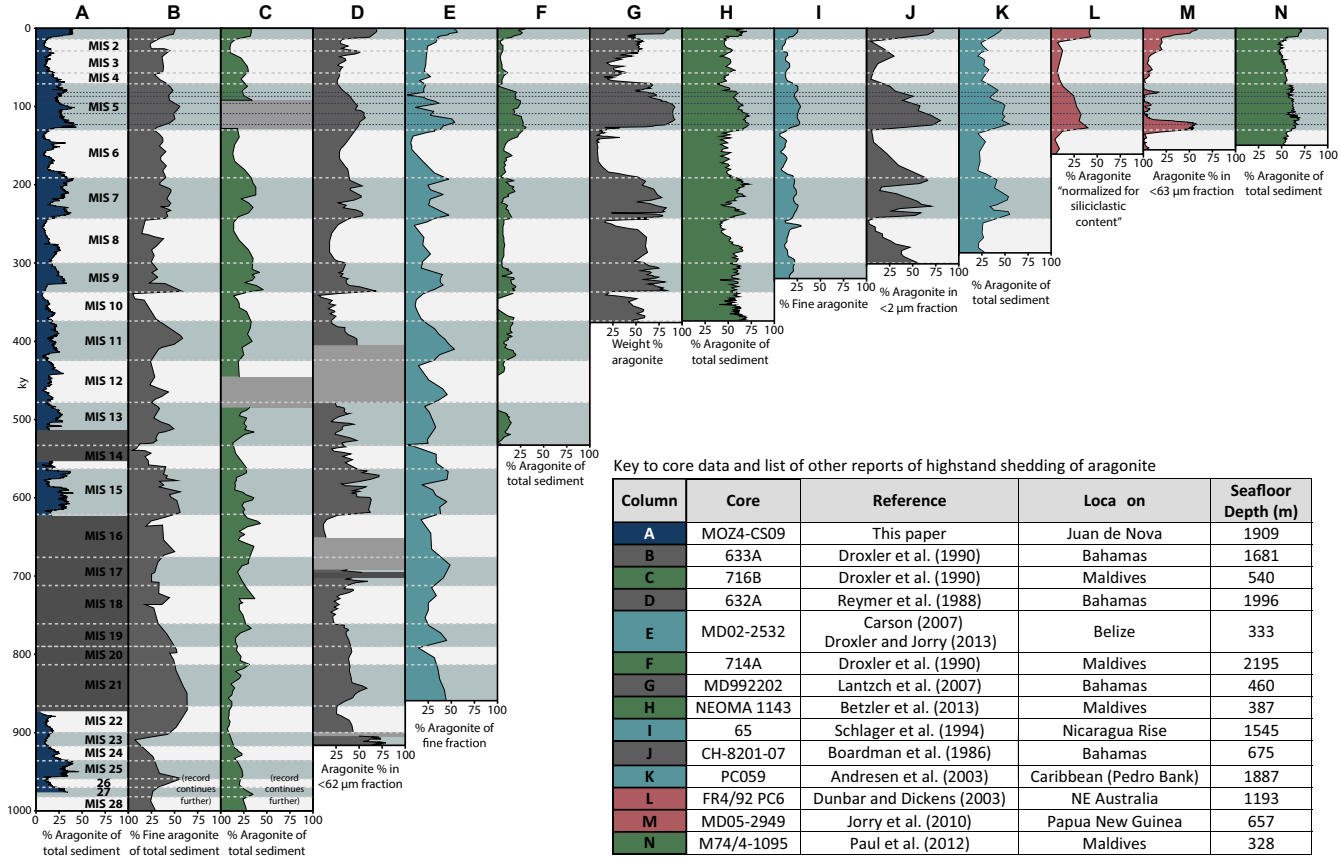

Key to core data and list of other reports of highstand shedding of aragonite

Column	Core	Reference	Loca on	Seafloor Depth (m)
A	MOZ4-CS09	This paper	Juan de Nova	1909
B	633A	Droxler et al. (1990)	Bahamas	1681
C	716B	Droxler et al. (1990)	Maldives	540
D	632A	Reymer et al. (1988)	Bahamas	1996
E	MD02-2532	Carson (2007) Droxler and Jorry (2013)	Belize	333
F	714A	Droxler et al. (1990)	Maldives	2195
G	MD992202	Lantzch et al. (2007)	Bahamas	460
H	NEOMA 1143	Betzler et al. (2013)	Maldives	387
I	65	Schlager et al. (1994)	Nicaragua Rise	1545
J	CH-8201-07	Boardman et al. (1986)	Bahamas	675
K	PC059	Andresen et al. (2003)	Caribbean (Pedro Bank)	1887
L	FR4/92 PC6	Dunbar and Dickens (2003)	NE Australia	1193
M	MD05-2949	Jorry et al. (2010)	Papua New Guinea	657
N	M74/4-1095	Paul et al. (2012)	Maldives	328

FIGURE 9 Comparison of the aragonite records of 13 global localities with that of Juan de Nova. Aragonite curves redrafted from publications listed in table, except for E and M, where only aragonite mass accumulation rates have been published and aragonite content was back-calculated. Each record is presented on its originally published age model; conversion of original low-resolution raster data into the form shown here may introduce additional error. This compilation should therefore not be used to analyse the exact timing and magnitude of aragonite content changes in detail, but is instead meant to illustrate larger scale trends

which is characterized by exceptionally high sea-levels (≤20 m above present, 13–20 m above present, or 6–13 m above present, according to Kindler and Hearty (2000), Droxler et al. (2003), and Dutton et al. (2015), respectively). In the Juan de Nova core, aragonite content during this time is on average lower than all other interglacial periods observed (Figures 5 and 7c), which may be a product of this larger dissolution supercycle. Evidence of dissolution can be seen in the sediments here in the form of pitting on the surface of aragonite needles (Figure 4b, 1410 cm). Alternatively, the diminished aragonite response on Juan de Nova may be due to a reduction in carbonate productivity because of drowning of the platform; sea-level during MIS 11 in particular may have been higher than present by up to 20 m (Kindler & Hearty, 2000), perhaps enough to incipiently drown the platform below its optimal productivity zone and reduce carbonate production. Aragonite content remains high, however, during MIS 5e, which was characterized by similarly warm temperatures and high sea-levels, suggesting that dissolution may be more likely.

5.4 | Comparison with highstand shedding elsewhere

In the Gulf of Papua and the northeastern shelf of Australia, mixed-system rimmed carbonate shelves have been shown to have a more complex relationship with sea-level than simple highstand shedding. In these cases, carbonate export was shown to peak during regression or transgression (Harper et al., 2015; Page & Dickens, 2005, respectively). In Juan de Nova, this is not usually the case—for most intervals, trends in aragonite content generally follow the sea-level curve. Once the platform floods during transgression, as mentioned above, subsequent aragonite peaks are generally coincident with maximum highstand. This suggests that carbonate production and export are dependent more on the water depth of the platform top rather than the trajectory of sea-level change. This "classical" type of highstand shedding has also been documented in a number of other localities around the globe.

Evidence for highstand shedding in carbonates elsewhere has taken the form of either: (a) changes in the frequency, thickness or changes in lithology of turbidite deposition in adjacent basins (Bernet, Eberli, & Gilli, 2000; Betzler, Pfeiffer, & Saxena, 2000; Haak & Schlager, 1989; Reijmer & Andresen, 2007; Reijmer, Palmieri, Groen, & Floquet, 2015; Reijmer et al., 2012), (b) differing sediment composition of highstand versus lowstand deposits (Grammer & Ginsburg, 1992), or (c) fine-grained aragonite export during highstand (Paul et al., 2012). Highstand shedding of fine-grained carbonate mud, as seen here, has been observed in numerous other localities (Figure 9 and references therein), with most records substantially shorter than the one reported here. The longest core records showing this trend, extending over 2 Myr (truncated in Figure 9b,c), are from IODP expeditions in the Bahamas and the Maldives (Droxler et al., 1990; Reymer et al., 1988). The record from JDN discussed here is the longest in the southern Indian Ocean, and because of the quantitative core scanning method used, it provides a higher level of detail than most other records (Figure 9). Like the core described here, each of the cores in these previous studies shows a sharp increase in aragonite content at the beginning of Stages 1, 5, 7 and 9, marking the flooding of each respective platform or shelf. The muted aragonite response during MIS 11 is most obvious in the Juan de Nova core and in the nearby Maldives (column C), suggesting the proposed aragonite dissolution supercycle operating during this time may have been more intense in the Indian Ocean. Although the mid-Brunhes event around MIS 11 marks a fundamental change in the amplitude of glacial–interglacial cycles on some other records (Holden, Edwards, Wolff, Valdes, & Singarayer, 2011), the magnitude of aragonite responses in Juan de Nova, the Maldives and the Bahamas during MIS 13 and 15 is not appreciably different than later interglacial periods (Droxler et al., 1990, 2003; Reymer et al., 1988). Later stages (MIS 22 and earlier), however, do not have the same clear correlation with glacial–interglacial cycles. While a general comparison can be made with these previously described records, the inherent error due to the lower resolutions, variable aragonite calculation methods, and different age models used in each study prevent a detailed comparison of the precise timing and magnitude of aragonite content changes. In addition, other cores were recovered at differing distances from their respective platforms, and each adjacent platform lies at a different depth, so the exact sedimentary response would be expected to differ slightly between records.

6 | CONCLUSIONS

Deep-sea sediments from a 27 m piston core near Juan de Nova island are characterized by cyclical variations in aragonite content that correspond to Late Quaternary glacial–interglacial episodes. These deposits are interpreted as being the product of highstand shedding, where carbonate sediments (in the form of fine-grained aragonite mud) are produced and exported from the top of the nearby Juan de Nova platform during interglacial intervals. Greenhouse conditions during these times result in higher sea-level, which floods the shallow platform and triggers increased carbonate production. Platform muds are then winnowed and transported off-platform in suspension, where they are redeposited in the deep sea. The core records discussed here show a new occurrence of this phenomenon in a region where it has not previously been documented. In addition, the Juan de Nova record is exceptional in its resolution and length when compared to most other documented instances of highstand shedding. Analysis of platform flooding windows suggests that little appreciable net subsidence or aggradation of the edifice has occurred in the past 1 Myr; these processes were likely balanced, keeping the height of the platform at relatively the same level. The new record is consistent with past hypotheses of increased sea floor dissolution of aragonite around MIS 11, supporting the idea that dissolution cycles affected the southern Indian Ocean. These results further confirm the recurrence of highstand shedding across time and space, as many other localities around the world have been shown to share a similar aragonite response to sea-level. This study underscores the importance of highstand shedding as a mechanism of carbonate transfer to the deep sea throughout the Late Quaternary, and therefore an important global control on sedimentation.

ACKNOWLEDGEMENTS

The oceanographic expeditions PTOLEMEE and PAMELA-MOZ4 were co-funded by TOTAL and IFREMER as part of the PAMELA (Passive Margin Exploration Laboratory; 13/1210499) scientific project. The REEFCORES project was supported by France's "Iles Eparses" program (2011–2014) managed by CNRS-InEE (Institut Ecologie et Environnement). This work was supported by the "Laboratoire d'Excellence" LabexMER (ANR-10-LABX-19) and co-funded by a grant from the French Government under the program "Investissements d'Avenir," and by a grant from the Regional Council of Brittany (SAD programme). We thank the Captain and the crew of the R/Vs *L'Atalante* and *Pourquoi pas?*, as well as the scientific participants in the PTOLEMEE and PAMELA-MOZ04 survey. Thanks also to Nils Andersen at Kiel University for isotope work, Nicolas Gayet for help with SEM images, Bernard Dennielou, Angélique Roubi, Deborah Belleney and Julian Vallet for the core analysis at the IFREMER sediment analysis laboratory. A final thank you to Prof. John Reijmer, an anonymous reviewer, and Associate Editor Sam Purkis for helpful comments and suggestions, which improved this manuscript greatly.

CONFLICT OF INTEREST

The authors declare no conflicts of interest.

ORCID

John W. Counts http://orcid.org/0000-0001-7374-6928
Stephan J. Jorry http://orcid.org/0000-0001-8240-9042
Natalia Vazquez Riveiros http://orcid.org/0000-0001-7513-153X
Gwenael Jouet http://orcid.org/0000-0002-2178-2115
Jacques Giraudeau http://orcid.org/0000-0002-5069-4667
Sandrine Cheron http://orcid.org/0000-0001-5876-8539
Audrey Boissier http://orcid.org/0000-0001-7979-3469
Elda Miramontes http://orcid.org/0000-0001-5968-9277

REFERENCES

Andresen, N., Reijmer, J. J. G., & Droxler, A. W. (2003). Timing and distribution of calciturbidites around a deeply submerged carbonate platform in a seismically active setting (Pedro Bank, Northern Nicaragua Rise, Caribbean Sea). *International Journal of Earth Sciences*, *92*, 573–592. https://doi.org/10.1007/s00531-003-0340-0

Bernet, K. H., Eberli, G. P., & Gilli, A. (2000). Turbidite frequency and composition in the distal part of the Bahamas transect. *Proceedings of the Ocean Drilling Program, Scientific Results*, *166*, 45–60.

Betzler, C., Lüdmann, T., Hübscher, C., & Fürstenau, J. (2013). Current and sea-level signals in periplatform ooze (Neogene, Maldives, Indian Ocean). *Sedimentary Geology*, *290*, 126–137. https://doi.org/10.1016/j.sedgeo.2013.03.011

Betzler, C., Pfeiffer, M., & Saxena, S. (2000). Carbonate shedding and sedimentary cyclicities of a distally steepened carbonate ramp (Miocene, Great Bahama Bank). *International Journal of Earth Sciences*, *89*, 140–153. https://doi.org/10.1007/s005310050322

Boardman, M. R., Neumann, A. C., Baker, P. A., Dulin, L. A., Kenter, R. J., Hunter, G. E., & Kiefer, K. B. (1986). Banktop responses to Quaternary fluctuations in sea level recorded in periplatform sediments. *Geology*, *14*, 28–31. https://doi.org/10.1130/0091-7613(1986) 14<28:BRTQFI>2.0.CO;2

Bosscher, H., & Schlager, W. (1992). Computer simulation of reef growth. *Sedimentology*, *39*, 503–512. https://doi.org/10.1111/j.1365-3091.1992.tb02130.x

Camoin, G. F., Montaggioni, L. F., & Braithwaite, C. J. R. (2004). Late glacial to post glacial sea levels in the Western Indian Ocean. *Marine Geology*, *206*, 119–146. https://doi.org/10.1016/j.margeo.2004.02.003

Carson, B. E. (2007). *Late Quaternary sediment accumulations and foraminiferal populations on the slopes of Gladden Basin (offshore Belize) and southern Ashmore Trough (Gulf of Papua) mixed siliciclastic-carbonate systems*. Doctoral dissertation, Rice University, 165 p.

Chabaud, L., Ducassou, E., Tournadour, E., Mulder, T., Reijmer, J. J., Conesa, G., & Ross, L. (2016). Sedimentary processes determining the modern carbonate periplatform drift of Little Bahama Bank. *Marine Geology*, *378*, 213–229. https://doi.org/10.1016/j.margeo.2015.11.006Get

Chéron, S., Etoubleau, J., Bayon, G., Garziglia, S., & Boissier, A. (2016). Focus on sulfur count rates along marine sediment cores acquired by XRF Core Scanner. *X-Ray Spectrometry*, *45*, 288–298. https://doi.org/10.1002/xrs.2704

Cohen, K. M., & Gibbard, P. (2008). Global chronostratigraphical correlation table for the last 2.7 million years. *Episodes*, *31*, 243–247.

Conrad Neumann, A. C., & Land, L. S. (1975). Lime mud deposition and calcareous algae in the Bight of Abaco, Bahamas; a budget. *Journal of Sedimentary Petrology*, *45*, 763–786. https://doi.org/10.1306/212F6E3D-2B24-11D7-8648000102C1865D

Counts, J. W., Jorry, S. J., Leroux, E., Miramontes, E., & Jouet, G. (2018). Sedimentation adjacent to atolls and volcano-cored carbonate platforms in the Mozambique Channel (SW Indian Ocean). *Marine Geology*, *404*, 41–59. https://doi.org/10.1016/j.margeo.2018.07.003

Courgeon, S., Jorry, S. J., Camoin, G. F., BouDagher-Fadel, M. K., Jouet, G., Révillon, S., … Droxler, A. W. (2016). Growth and demise of Cenozoic isolated carbonate platforms: New insights from the Mozambique Channel seamounts (SW Indian Ocean). *Marine Geology*, *380*, 90–105. https://doi.org/10.1016/j.margeo.2016.07.006

Dravis, J. J. (1996). Rapidity of freshwater calcite cementation—Implications for carbonate diagenesis and sequence stratigraphy. *Sedimentary Geology*, *107*, 1–10. https://doi.org/10.1016/S0037-0738(96)00063-2

Droxler, A. W., Alley, R. B., Howard, W. R., Poore, R. Z., & Burckle, L. H. (2003). Unique and exceptionally long interglacial Marine Isotope Stage 11: Window into Earth warm future climate. In A. W. Droxler, R. Z. Poore, & L. H. Burckle (Eds.), *Earth's climate and orbital eccentricity: The marine isotope stage 11 question* (pp. 1–14). Geophysical Monograph Series, 137. Washington, DC: American Geophysical Union. https://doi.org/10.1029/137gm01

Droxler, A. W., Haddad, G. A., Mucciarone, D. A., & Cullen, J. L. (1990). 29. Pliocene-Pleistocene aragonite cyclic variations in holes 714a and 716b (the Maldives) compared with hole 633a (the Bahamas): Records of climate-induced $CaCO_3$ preservation at intermediate water depths. In R. A. Duncan, J. Backman, R. B. Dunbar, & L. C. Peterson, (Eds.), *Proceedings of the ocean drilling program, scientific results* (Vol. 115, pp. 539–577). College Station, Texas: Ocean Drilling Program.

Droxler, A. W., & Jorry, S. J. (2013). Deglacial origin of barrier reefs along low-latitude mixed siliciclastic and carbonate continental shelf edges. *Annual Review of Marine Science*, *5*, 165–190. https://doi.org/10.1146/annurev-marine-121211-172234

Droxler, A. W., & Schlager, W. (1985). Glacial versus interglacial sedimentation rates and turbidite frequency in the Bahamas. *Geology*, *13*, 799–802. https://doi.org/10.1130/0091-7613(1985) 13<799:GVISRA>2.0.CO;2

Droxler, A. W., Schlager, W., & Whallon, C. C. (1983). Quaternary aragonite cycles and oxygen-isotope record in Bahamian carbonate ooze. *Geology*, *11*, 235–239. https://doi.org/10.1130/0091-7613(1983) 11<235:QACAOR>2.0.CO;2

Dunbar, G. B., & Dickens, G. R. (2003). Late Quaternary shedding of shallow-marine carbonate along a tropical mixed siliciclastic–carbonate shelf: Great Barrier Reef, Australia. *Sedimentology*, *50*, 1061–1077. https://doi.org/10.1046/j.1365-3091.2003.00593.x

Dutton, A., Bard, E., Antonioli, F., Esat, T. M., Lambeck, K., & McCulloch, M. T. (2009). Phasing and amplitude of sea-level and climate change during the penultimate interglacial. *Nature Geoscience*, *2*, 355–359. https://doi.org/10.1038/ngeo470

Dutton, A., Carlson, A. E., Long, A. J., Milne, G. A., Clark, P., DeConto, R., & Raymo, M. E. (2015). Sea-level rise due to polar ice-sheet mass loss during past warm periods. *Science*, *349*, 4019. https://doi.org/10.1126/science.aaa4019

Emmermann, P. (2000). *Mineralogy, geochemistry and microfacies of Late Quaternary periplatform sediments: Carbonate export cycles and secondary processes-Sanganeb Atoll and Abington Reef, Sudan, Central Red Sea*. Doctoral dissertation, University of Kiel, 169 p.

Everts, A. J. (1991). Interpreting compositional variations of calciturbidites in relation to platform-stratigraphy: An example from the Paleogene of SE Spain. *Sedimentary Geology*, *71*, 231–242. https://doi.org/10.1016/0037-0738(91)90104-L

Fontanier, C., Mamo, B., Toucanne, S., Bayon, G., Schmidt, S., Deflandre, B., & Jorry, S. J. (2018). Are deep-sea ecosystems surrounding Madagascar threatened by land-use or climate change? *Deep-Sea Research Part I-Oceanographic Research Papers*, *131*, 93–100. https://doi.org/10.1016/j.dsr.2017.11.011

Giraudeau, J., Christensen, B. A., Hermelin, O., Lange, C. B., Motoyama, I.; Shipboard Scientific Party. (1998). Biostratigraphic age models and sedimentation rates along the southwest African margin. In G. Wefer, W. H. Berger, & C. Richter (Eds.), *Proceedings of the ocean drilling program initial reports* (Vol. 175, pp. 543–546). College Station, Texas: Ocean Drilling Program.

Glaser, K. S., & Droxler, A. W. (1991). High production and highstand shedding from deeply submerged carbonate banks, northern Nicaragua Rise. *Journal of Sedimentary Research*, *61*, 128–142. https://doi.org/10.1306/D42676A4-2B26-11D7-8648000102C1865D

Glaser, K. S., & Droxler, A. W. (1993). Controls and development of Late Quaternary periplatform carbonate stratigraphy in Walton Basin (northeastern Nicaragua Rise, Caribbean Sea). *Paleoceanography*, *8*, 243–274. https://doi.org/10.1029/92PA02876

Grammer, G. M., & Ginsburg, R. N. (1992). Highstand versus lowstand deposition on carbonate platform margins: Insight from Quaternary foreslopes in the Bahamas. *Marine Geology*, *103*, 125–136. https://doi.org/10.1016/0025-3227(92)90012-7

Haak, A. B., & Schlager, W. (1989). Compositional variations in calciturbidites due to sea-level fluctuations, Late Quaternary, Bahamas. *Geologische Rundschau*, *78*, 477–486. https://doi.org/10.1007/BF01776186

Harper, B. B., Puga-Bernabéu, Á., Droxler, A. W., Webster, J. M., Gischler, E., Tiwari, M., & Röhl, U. (2015). Mixed carbonate–siliciclastic sedimentation along the great barrier reef upper slope: A challenge to the reciprocal sedimentation model. *Journal of Sedimentary Research*, *85*, 1019–1036. https://doi.org/10.2110/jsr.2015.58.1

Hine, A. C., Wilber, R. J., Bane, J. M., Neumann, A. C., & Lorenson, K. R. (1981). Offbank transport of carbonate sands along open, leeward bank margins: Northern Bahamas. *Marine Geology*, *42*, 327–348. https://doi.org/10.1016/0025-3227(81)90169-9

Hodell, D. A., Channell, J. E., Curtis, J. H., Romero, O. E., & Röhl, U. (2008). Onset of "Hudson Strait" Heinrich events in the eastern North Atlantic at the end of the middle Pleistocene transition (~640 ka)? *Paleoceanography*, *23*, 1–16. https://doi.org/10.1029/2008PA001591

Holden, P. B., Edwards, N. R., Wolff, E. W., Valdes, P. J., & Singarayer, J. S. (2011). The Mid-Brunhes event and West Antarctic ice sheet stability. *Journal of Quaternary Science*, *26*, 474–477. https://doi.org/10.1002/jqs.1525

Jorry, S. J. (2014). *PTOLEMEE cruise, RV L'Atalante*. https://doi.org/10.17600/14000900

Jorry, S. J., Camoin, G. F., Jouet, G., Le Roy, P., Vella, C., Courgeon, S., & Caline, B. (2016). Modern sediments and Pleistocene reefs from isolated carbonate platforms (Iles Eparses, SW Indian Ocean): A preliminary study. *Acta Oecologica*, *72*, 129–143. https://doi.org/10.1016/j.actao.2015.10.014

Jorry, S. J., Droxler, A. W., & Francis, J. M. (2010). Deepwater carbonate deposition in response to re-flooding of carbonate bank and atoll-tops at glacial terminations. *Quaternary Science Reviews*, *29*, 17–18. https://doi.org/10.1016/j.quascirev.2010.04.016

Jouet, G., & Deville, E. (2015) *PAMELA-MOZ04 cruise, RV Pourquoi Pas?* https://doi.org/10.17600/15000700

Kindler, P., & Hearty, P. J. (2000). Elevated marine terraces from Eleuthera (Bahamas) and Bermuda: Sedimentological, petrographic and geochronological evidence for important deglaciation events during the middle Pleistocene. *Global and Planetary Change*, *24*, 41–58. https://doi.org/10.1016/S0921-8181(99)00068-5

Lantzsch, H., Roth, S., Reijmer, J. J., & Kinkel, H. (2007). Sea-level related resedimentation processes on the northern slope of Little Bahama Bank (Middle Pleistocene to Holocene). *Sedimentology*, *54*, 1307–1322. https://doi.org/10.1111/j.1365-3091.2007.00882.x

Lisiecki, L. E., & Raymo, M. E. (2005). A Pliocene-Pleistocene stack of 57 globally distributed benthic δ18O records. *Paleoceanography*, *20*, 1–17. https://doi.org/10.1029/2004PA001071

Macintyre, I. G., & Reid, R. P. (1992). Comment on the origin of aragonite needle mud: A picture is worth a thousand words. *Journal of Sedimentary Research*, *62*, 1095–1097. https://doi.org/10.1306/D4267A5A-2B26-11D7-8648000102C1865D

Météo France. (2017). Retrieved from https://publitheque.mete.fr/Donnees/DESC1705311715640289.KEYu07f7D3UO9xudD2U2fU9.html1/2

Miller, K. G., Mountain, G. S., Wright, J. D., & Browning, J. V. (2011). A 180-million-year record of sea level and ice volume variations from continental margin and deep-sea isotopic records. *Oceanography*, *24*, 40–53. https://doi.org/10.5670/oceanog.2011.26

Milliman, J. D., Freile, D., Steinen, R. P., & Wilber, R. J. (1993). Great Bahama Bank aragonitic muds: Mostly inorganically precipitated, mostly exported. *Journal of Sedimentary Research*, *63*, 589–595. https://doi.org/10.1306/D4267B81-2B26-11D7-8648000102C1865D

Milliman, J. D., Müller, G., & Förstner, F. (1974). *Recent sedimentary carbonates: Part 1 marine carbonates*. New York, NY: Springer Science & Business Media.

Page, M. C., & Dickens, G. R. (2005). Sediment fluxes to Marion Plateau (southern Great Barrier Reef province) over the last 130 ky: New constraints on 'transgressive-shedding'off northeastern Australia. *Marine Geology*, *219*, 27–45. https://doi.org/10.1016/j.margeo.2005.05.002

Paillard, D., Labeyrie, L. D., & Yiou, P. (1996). AnalySeries 1.0: A Macintosh software for the analysis of geophysical time-series. *Eos*, *77*, 123–152.

Paul, A., Reijmer, J. J. G., Fürstenau, J., Kinkel, H., & Betzler, C. (2012). Relationship between Late Pleistocene sea-level variations, carbonate platform morphology and aragonite production (Maldives, Indian Ocean). *Sedimentology*, *59*, 1640–1658. https://doi.org/10.1111/j.1365-3091.2011.01319.x

Perry, C. T., Salter, M. A., Harborne, A. R., Crowley, S. F., Jelks, H. L., & Wilson, R. W. (2011). Fish as major carbonate mud producers and missing components of the tropical carbonate factory. *Proceedings*

of the National Academy of Sciences of the United States of America, *108*, 3865–3869. https://doi.org/10.1073/pnas.1015895108

Prat, S., Jorry, S. J., Jouet, G., Camoin, G., Vella, C., Le Roy, P., & Pastol, Y. (2016). Geomorphology and sedimentology of a modern isolated carbonate platform: The Glorieuses archipelago, SW Indian Ocean. *Marine Geology*, *380*, 272–283. https://doi.org/10.1016/j.margeo.2016.04.009

Pujos, A. (1988). Spatio-temporal distribution of some Quaternary coccoliths. *Oceanologica Acta*, *11*, 65–77.

Reale, V., & Monechi, S. (2005). Distribution of the calcareous nannofossil *Reticulofenestra asanoi* within the early-middle Pleistocene transition in the Mediterranean Sea and Atlantic Ocean: Correlation with magneto-and oxygen isotope stratigraphy. *Geological Society, London, Special Publications*, *247*, 117–130. https://doi.org/10.1144/GSL.SP.2005.247.01.06

Reijmer, J. J., & Andresen, N. (2007). Mineralogy and grain size variations along two carbonate margin-to-basin transects (Pedro Bank, Northern Nicaragua Rise). *Sedimentary Geology*, *198*, 327–350. https://doi.org/10.1016/j.sedgeo.2007.01.018

Reijmer, J. J. G., Palmieri, P., & Groen, R. (2012). Compositional variations in calciturbidites and calcidebrites in response to sea-level fluctuations (Exuma Sound, Bahamas). *Facies*, *58*, 493–507. https://doi.org/10.1007/s10347-011-0291-z

Reijmer, J. J. G., Palmieri, P., Groen, R., & Floquet, M. (2015). Calciturbidites and calcidebrites: Sea-level variations or tectonic processes? *Sedimentary Geology*, *317*, 53–70. https://doi.org/10.1016/j.sedgeo.2014.10.013

Reijmer, J. J. G., Ten Kate, W. G. H. Z., Sprenger, A., & Schlager, W. (1991). Calciturbidite composition related to exposure and flooding of a carbonate platform (Triassic, Eastern Alps). *Sedimentology*, *38*, 1059–1074. https://doi.org/10.1111/j.1365-3091.1991.tb00371.x

Rendle-Bühring, R. H., & Reijmer, J. J. G. (2005). Controls on grain-size patterns in periplatform carbonates: Marginal setting versus glacio-eustacy. *Sedimentary Geology*, *175*, 99–113. https://doi.org/10.1016/j.sedgeo.2004.12.025

Reymer, J. J. G., Schlager, W., & Droxler, A. W. (1988). 15. Site 632: Pliocene-Pleistocene sedimentation cycles in a Bahamian basin. In J. A. Austin, Jr. & W. Schlager, et al. (Eds), *Proceedings of the ocean drilling program: Bahamas: Covering Leg 101 of the cruises of the drilling vessel JOIDES resolution, Miami, Florida, to Miami, Florida, Sites 626–636, 29 January, 1985–14 March, 1985. Scientific results* (Vol. 101, pp. 213–220). College Station, Texas: Ocean Drilling Program.

Sætre, R. (1985). Surface currents in the Mozambique Channel. Deep sea research part A. *Oceanographic Research Papers*, *32*, 1457–1467. https://doi.org/10.1016/0198-0149(85)90097-4

Salter, M. A., Perry, C. T., Stuart-Smith, R. D., Edgar, G. J., Wilson, R. W., & Harborne, A. R. (2018). Reef fish carbonate production assessments highlight regional variation in sedimentary significance. *Geology*, *46*, 699–702. https://doi.org/10.1130/G45286.1

Sato, T., Kameo, K., & Takayama, T. (1991). Coccolith biostratigraphy of the Arabian sea. In W. L. Prell & N. Niitsuma, et al. (Eds.), *Proceedings of the ocean drilling program. Scientific results, Oman Margin/Neogene Package: Covering Leg 117 of the cruises of the drilling vessel JOIDES resolution, Port Louis, Mauritius, to Port Louis, Mauritius, Sites 720–731, 19 August 1987–17 October 1987* (Vol. 117, pp. 37–54). College Station, Texas: Ocean Drilling Program.

Schlager, W., Reijmer, J. J. G., & Droxler, A. W. (1994). Highstand shedding of carbonate platforms. *Journal of Sedimentary Research*, *64*, 270–281. https://doi.org/10.1306/D4267FAA-2B26-11D7-8648000102C1865D

Schlanger, S. O. (1988). Strontium storage and release during deposition and diagenesis of marine carbonates related to sea-level variations. In A. Lerman & M. Meybeck (Eds.), *Physical and chemical weathering in geochemical cycles* (pp. 323–339). Dordrecht, The Netherlands: Kluwer Academic.

Schott, F. A., Xie, S. P., & McCreary, J. P. (2009). Indian Ocean circulation and climate variability. *Reviews of Geophysics*, *47*, 1–46. https://doi.org/10.1029/2007RG000245

Sepulcre, S., Durand, N., & Bard, E. (2017). Large ^{14}C age offsets between the fine fraction and coexisting planktonic foraminifera in shallow Caribbean sediments. *Quaternary Geochronology*, *38*, 61–74. https://doi.org/10.1016/j.quageo.2016.12.002

Spratt, R. M., & Lisiecki, L. E. (2016). A late Pleistocene sea level stack. *Climate of the Past*, *12*, 1079–1092. https://doi.org/10.5194/cp-12-1079-2016

Strasser, A., & Samankassou, E. (2003). Carbonate sedimentation rates today and in the past: Holocene of Florida Bay, Bahamas, and Bermuda vs. Upper Jurassic and Lower Cretaceous of the Jura Mountains (Switzerland and France). *Geologia Croatica*, *56*, 1–18.

Thierstein, H. R., Geitzenauer, K., Molfino, B., & Shackleton, N. J. (1977). Global synchroneity of Late Quaternary coccolith datum levels: Validation by oxygen isotopes. *Geology*, *5*, 400–404. https://doi.org/10.1130/0091-7613(1977)5%3C400:GSOLQC%3E2.0.CO;2

Vecsei, A., & Sanders, D. G. (1997). Sea-level highstand and lowstand shedding related to shelf margin aggradation and emersion, upper Eocene-Oligocene of Maiella carbonate platform, Italy. *Sedimentary Geology*, *112*, 219–234. https://doi.org/10.1016/S0037-0738(97)00044-4

Weaver, P. P. E. (1993). High resolution stratigraphy of marine Quaternary sequences. *Geological Society, London, Special Publications*, *70*, 137–153. https://doi.org/10.1144/GSL.SP.1993.070.01.10

Wilson, P. A., & Roberts, H. H. (1995). Density cascading: Off-shelf sediment transport, evidence and implications, Bahama Banks. *Journal of Sedimentary Research*, *65*, 45–56. https://doi.org/10.1306/D426801D-2B26-11D7-8648000102C1865D

Zinke, J., Reijmer, J. J. G., Thomassin, B. A., Dullo, W. C., Grootes, P. M., & Erlenkeuser, H. (2003). Postglacial flooding history of Mayotte lagoon (Comoro archipelago, southwest Indian Ocean). *Marine Geology*, *194*, 181–196. https://doi.org/10.1016/S0025-3227(02)00705-3

SUPPORTING INFORMATION

Additional supporting information may be found online in the Supporting Information section at the end of the article.

How to cite this article: Counts JW, Jorry SJ, Vazquez Riveiros N, et al. A Late Quaternary record of highstand shedding from an isolated carbonate platform (Juan de Nova, southern Indian Ocean). *Depositional Rec*. 2019;5:540–557. https://doi.org/10.1002/dep2.57